

Robust dynamic decoupling control for permanent magnet spherical actuators based on extended state observer

Jingmeng Liu¹, Huiyang Deng¹, Weihai Chen¹✉, Shaoping Bai²

¹Automation Science and Electrical Engineering, Beihang University, BeiHang University XueYuan Road No. 37, HaiDian District, BeiJing, People's Republic of China

²Engineering and Science, Aalborg University, Aalborg, Denmark

✉ E-mail: whchenbuua@126.com

ISSN 1751-8644

Received on 19th May 2016

Revised 5th November 2016

Accepted on 27th November 2016

doi: 10.1049/iet-cta.2016.0551

www.ietdl.org

Abstract: This study presents a robust dynamic decoupling control strategy to solve the trajectory tracking problem for the permanent magnet spherical actuator (PMSA). The dynamic model of PMSA obtained by the Lagrange–Euler formalism is obviously a multi-variable non-linear system with strong cross-couplings. Furthermore, uncertainties such as model errors and external disturbances will also affect the precision of the control system. In the active disturbance rejection control (ADRC) framework, the decoupling problem can be reformulated as disturbance rejection by merging the cross channel interference into the lumped disturbance, which consists of internal dynamics and external disturbances. The lumped disturbance is then estimated using extended state observer (ESO) and canceled out in the control law. Herein, the linear active disturbance rejection control is selected for PMSAs, as the tuning process can be greatly simplified by making all the parameters of ESO or controller a function of bandwidth. Simulations and experiments are presented to corroborate the effectiveness and robustness of the proposed strategy, showing that the proposed control algorithm can decouple and linearise the system in the presence of model errors as well as the load and random disturbances. Meanwhile, the modified system has better static and dynamic performances with strong robustness to uncertainties.

Notations

q	Euler angle vector used to express the rotor orientation
$M(q)$	inertial matrix of PMSA
$C(\dot{q}, q)$	Coriolis force coefficient matrix of PMSA
J_i	principal inertial moments of the i th axis
τ_c	vector of control torques
τ_d	vector of external disturbances
τ_l	vector of load torques
τ_r	vector of random torques
$\hat{x}_{j,\alpha}$	estimated value of the state variable in the X -axis
$x_{j,\alpha}$	actual value of the state variable in the X -axis
$r_{j,\alpha}$	reference value of angle or velocity in the X -axis
$e_{j,\alpha}$	tracking error of the state variable in the X -axis
$E_{j,\alpha}$	tracking error of angle or velocity in the X -axis
$\omega_{c,i}$	bandwidth of the controller in the i th channel
$\omega_{o,i}$	bandwidth of ESO in the i th channel
T	vector of torque obtained from current
G	torque matrix
I	vector of current
w	vector of external disturbance
U	vector of actual control input
V	vector of virtual control input
f_i	the lumped disturbance in the i th channel
$[A]_j$	the j th row of matrix A
$[A]_{jk}$	the element in the j th row and k th column of matrix A
$ A $	the absolute value of A which means replacing each element of matrix A with its absolute value

1 Introduction

Many industrial applications such as robotic joints, automobile wheels or underwater vehicles involve orientation control of the rotating shaft. Conventionally, this type of motion is achieved by connecting a few single-axis actuators in series or in parallel with external mechanism. However, this combined actuation system has

intrinsic disadvantages, such as bulky structure, large backlash, slow dynamic response, singularity existence in workspace and lack of dexterity. To overcome these drawbacks, some novel concepts of spherical actuator, which can realise three degree-of-freedom (3-DOF) motion in one joint, have been proposed.

One concept is the ultrasonic spherical motor, which is based on the reverse piezoelectric [1, 2]. The advantage of this motor is its high resolution, while the shortcomings are small working range, complex fabrication and hysteresis. A spherical wheel motor, an alternative design of a variable reluctance spherical motor developed by Lee *et al.*, [3, 4] decouples the spin from the inclination. The permanent magnet spherical motor (PMSM), which has a four-pole spherical magnet rotor and four sets of stator, was introduced by Wang *et al.* [5]. Furthermore, Xia *et al.* presented a novel halbach array PMSM. By applying Halbach array to the PMSM, the magnetic field distribution is more sinusoidal, resulting in improving air gap field distribution and suppressing the torque ripple as well [6, 7]. In this paper, we focus on our own permanent magnet spherical actuator (PMSA) based on the electromagnetic principle [8], since it has many advantages such as small size, light weight, simple structure, high torque, low cost and so on.

A classical method to control PMSA is to use proportional derivative (PD) control law [9, 10]. It has the advantage of simplicity in design and implementation, which leads to acceptable results in many dynamic control areas [11–13]. Nevertheless, it can be inferred from the dynamics that PMSA is a system with complex non-linearity and strong couplings [4]. In addition, PMSAs are usually subject to model errors and external disturbances, hence the trajectory tracking performance of the PD control scheme will be seriously affected. To solve these problems, computed torque method has been widely used in the dynamic control of PMSA [14, 15]. While the control scheme linearises and decouples the dynamics to some extent, the performance is still not satisfactory in the presence of uncertainties. In [16, 17], artificial neural network has been applied to the spherical motor. However, a common back propagation algorithm is easy to fall into local minimum, and the advanced one with additional momentum

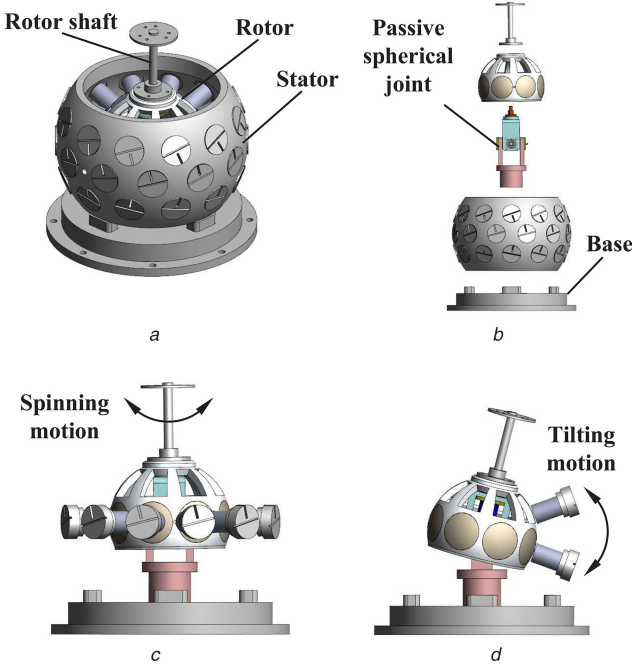


Fig. 1 Technical structure and the 3-DOF motion of PMSA
(a) CAD model, (b) Explosive view, (c) Spinning motion, (d) Tilting motion

demands extensive training data and a significant computational time, which brings challenges for real-time control. To cope with the uncertainties, iterative learning control is also proposed for PMSA [18]. Nevertheless, this method does not take the coupling terms into consideration and is dependent on multiple iterations, which limits its application for high-precision and intelligent control.

Considering all these matters, an advanced control strategy is required to linearise and decouple the dynamic model and enable PMSA to get high accuracy performance under uncertainties. It is noted that ADRC is an extended state observer (ESO)-based control (ESOBC) approach that has been applied in many areas, such as robotic systems [19, 20], motion control systems [21, 22] and flight control systems [23, 24]. Due to the fact that the dynamics of quadrotor helicopter and spherical motor are similar, so the control scheme of ADRC, which has been successfully used in the field of quadrotors [25, 26], is an excellent choice for PMSAs to improve their trajectory tracking performance. First, the cross-couplings, along with uncertainties such as modelling errors, loads and external disturbances, can be all treated as disturbances. In [27, 28], multi-variable systems are readily decoupled by estimating and rejecting the effects of both the internal plant dynamics and external disturbances through ESO. Second, ADRC is not a model-based control strategy, which requires least amount of plant information. Hence, it is very robust against parameter variations, disturbances and noise [29]. Although the identification of the lumped disturbance is operated online, it will not cause too

much calculating work compared with other methods, so the real time performance of the system can be improved significantly.

In this paper, the above ADRC framework has been introduced into the robust dynamic decoupling control of PMSA, which yields major contributions as follows:

- i. The coupling terms are divided into two class: the static couplings and the dynamic couplings. The static couplings among input-output pairs are solved by introducing the concept of virtual control input, while the dynamic couplings are included as part of the lumped disturbance, which can be observed by ESO.
- ii. The coupling terms, along with uncertainties such as model errors and external disturbances, constitute the lumped disturbance. Herein, ESO has been adopted to estimate the lumped disturbance online.
- iii. The bandwidth parameterisation has been introduced to adjust the parameters of both ESO and controller, simplifying the tuning process and reducing the computational time, which makes the practical application possible.

The reminder of this paper is organised as follows. Section 2 presents the dynamic model and torque model of PMSA. Section 3 first reformulates the decoupling problem by introducing the concept of static decoupling and dynamic decoupling, and then illustrates the design of both ESO and controller. Parameter setting and convergence analysis are given at the end of this section. Sections 4 and 5 present simulations and experiments, respectively. Finally, the concluding remarks are given in Section 6.

2 Dynamic and torque model of PMSA

The mechanical structure of PMSA is shown in Figs. 1a and b. It consists of a ball-shaped rotor with eight PM poles in one layer and a spherical-shell-like stator with 30 air-core coils in three layers. The rotor, supported by a passive spherical joint that contains an encoder and two potentiometers to measure the orientation, can realise tilting and spinning motion within working space. Specifically, as shown in Figs. 1c and d, the upper and lower coils, being symmetrically placed about the equatorial plane, are responsible for the tilting motion generated by the attraction or repulsion forces between the coils and permanent magnets, while the spinning motion is governed by the middle layer coils with a step control approach.

2.1 Dynamic modelling

Fig. 2a shows the definition of the stator coordinate, and the rotation matrix R_{rs} can be obtained through rotations around the axes of the stator coordinate (see Fig. 2b). Herein, $R_{rs} \in SO(3)$ is an orthonormal matrix. Euler angles are used to describe the rotor orientation, which are bounded as follows: tilting angle α, β , by $(-15^\circ < \alpha, \beta < 15^\circ)$ and spinning angle γ , by $(0^\circ < \gamma < 360^\circ)$.

The corresponding rotation matrix is as follows: (see equation below)

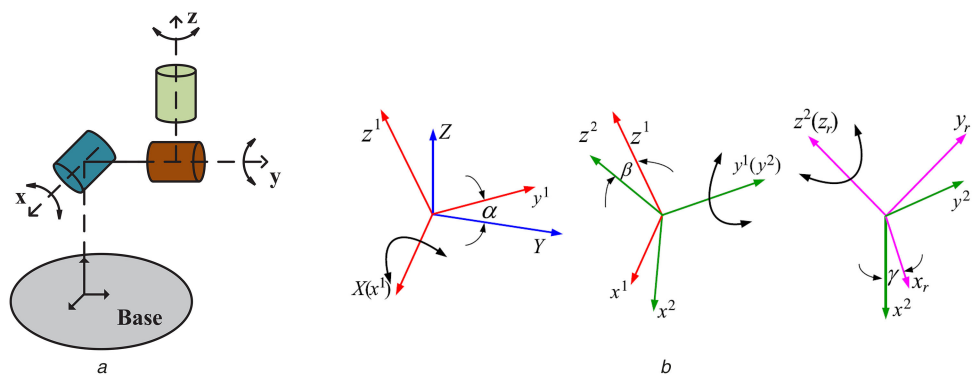


Fig. 2 Description of the position
(a) Coordinate definition, (b) Euler angles

The ideal dynamic model can be expressed by the Lagrange–Euler formalism based on the kinetic and potential energy concept as

$$M(q)\ddot{q} + C(\dot{q}, q)\dot{q} + N(\dot{q}, q) = \tau_c \quad (1)$$

where

$$q = [\alpha, \beta, \gamma]^T$$

and

$$M = \begin{bmatrix} m_{11} & m_{12} & m_{13} \\ m_{21} & m_{22} & m_{23} \\ m_{31} & m_{32} & m_{33} \end{bmatrix}$$

where

$$\begin{aligned} m_{11} &= J_1 \cos^2 \beta \cos^2 \gamma + J_2 \cos^2 \beta \sin^2 \gamma + J_3 \sin^2 \beta \\ m_{12} &= (J_1 - J_2) \cos \beta \cos \gamma \sin \gamma \\ m_{13} &= J_3 \sin \beta \\ m_{21} &= (J_1 - J_2) \cos \beta \cos \gamma \sin \gamma \\ m_{22} &= J_1 \sin^2 \gamma + J_2 \cos^2 \gamma \\ m_{23} &= 0 \\ m_{31} &= J_3 \sin \beta \\ m_{32} &= 0 \\ m_{33} &= J_3 \end{aligned}$$

and

$$C(\dot{q}, q) = \begin{bmatrix} c_{11} & c_{12} & c_{13} \\ c_{21} & c_{22} & c_{23} \\ c_{31} & c_{32} & c_{33} \end{bmatrix}$$

where (see equation below) and

$$N(\dot{q}, q) = 0 \quad (2)$$

From the above expression, the Lagrange–Euler rotational equation can be written in general form as follows:

$$M(q)\ddot{q} + C(\dot{q}, q)\dot{q} = \tau_c \quad (3)$$

where $M(q)$ and $C(\dot{q}, q)$ are the inertial and Coriolis force coefficient matrices, respectively. $q = [\alpha, \beta, \gamma]^T$ is the Euler angle vector, and $\tau_c = [\tau_\alpha, \tau_\beta, \tau_\gamma]^T$ is the vector of control torques. The principal inertial moments of the rotor are $J_1 = J_{xx}$, $J_2 = J_{yy}$ and $J_3 = J_{zz}$, respectively.

Considering the effect of uncertainties, the dynamic model (3) is modified as

$$\hat{M}(q)\ddot{q} + \hat{C}(\dot{q}, q)\dot{q} = \tau_c - \tau_d = \tau_c - \tau_l - \tau_r \quad (4)$$

where $\hat{M}(q) = M(q) + \Delta M(q)$ is the actual inertial matrix, $\hat{C}(\dot{q}, q) = C(\dot{q}, q) + \Delta C(\dot{q}, q)$ is the actual Coriolis matrix. Herein, $\Delta M(q)$ and $\Delta C(\dot{q}, q)$ are the model errors, which are caused by the estimation deviation of J_1 , J_2 and J_3 . $\tau_d = \tau_l + \tau_r$ denotes the external disturbances, containing load disturbance τ_l and random disturbance τ_r .

Therefore, the mathematical model (used for the controller synthesis) that describes the rotational movement of PMSA obtained from the Lagrange–Euler formalism is given by

$$\ddot{q} = -\hat{M}(q)^{-1}\hat{C}(\dot{q}, q)\dot{q} + \hat{M}(q)^{-1}(\tau_c - \tau_l - \tau_r) \quad (5)$$

2.2 Torque modelling

The torque model of the spherical motor is to establish the relationship between the current input of the stator coils and the

$$R_{rs} = \begin{bmatrix} \cos \beta \cos \gamma & -\cos \beta \sin \gamma & \sin \beta \\ \cos \gamma \sin \alpha \sin \beta + \cos \alpha \sin \gamma & \cos \alpha \cos \gamma - \sin \alpha \sin \beta \sin \gamma & -\cos \beta \sin \alpha \\ -\cos \gamma \sin \alpha \sin \beta + \sin \alpha \sin \gamma & \cos \gamma \sin \alpha + \cos \alpha \sin \beta \sin \gamma & \cos \alpha \cos \beta \end{bmatrix}$$

$$\begin{aligned} c_{11} &= (J_1 \cos \beta \sin \beta \cos^2 \gamma - J_2 \cos \beta \sin \beta \sin^2 \gamma + J_3 \sin \beta \cos \beta) \dot{\beta} \\ &\quad + (-J_1 \sin \gamma \cos \gamma \cos^2 \beta + J_2 \cos^2 \beta \sin \gamma \cos \gamma) \dot{\gamma} \\ c_{12} &= (-J_1 \cos \beta \sin \beta \cos^2 \gamma - J_2 \cos \beta \sin \beta \sin^2 \gamma + J_3 \sin \beta \cos \beta) \dot{\alpha} + ((J_1 - J_2) \sin \beta \sin \gamma \cos \gamma) \dot{\beta} \\ &\quad + \frac{1}{2}(-J_1 - J_2) \cos \beta \sin^2 \gamma + (J_1 - J_2) \cos \beta \cos^2 \gamma + J_3 \sin \beta \dot{\gamma} \\ c_{13} &= -((J_1 - J_2) \cos \gamma \sin \gamma \cos^2 \beta) \dot{\alpha} + \frac{1}{2}(-J_1 - J_2) \cos \beta \sin^2 \gamma \\ &\quad + (J_1 - J_2) \cos \beta \cos^2 \gamma + J_3 \cos \beta \dot{\beta} \\ c_{21} &= (J_1 \cos \beta \sin \beta \cos^2 \gamma + J_2 \cos \beta \sin \beta \sin^2 \gamma - J_3 \sin \beta \cos \beta) \dot{\alpha} \\ &\quad + \frac{1}{2}(-J_1 - J_2) \cos \beta \sin^2 \gamma + (J_1 - J_2) \cos \beta \cos^2 \gamma - J_3 \cos \beta \dot{\gamma} \\ c_{22} &= ((J_1 - J_2) \cos \gamma \sin \gamma) \dot{\gamma} \\ c_{23} &= \frac{1}{2}(-J_1 - J_2) \cos \beta \sin^2 \gamma + (J_1 - J_2) \cos \beta \cos^2 \gamma - J_3 \cos \beta \dot{\alpha} \\ &\quad + ((J_1 - J_2) \cos \gamma \sin \gamma) \dot{\beta} \\ c_{31} &= ((J_1 - J_2) \cos \gamma \sin \gamma \cos^2 \beta) \dot{\alpha} + \frac{1}{2}(J_1 - J_2) \cos \beta \sin^2 \gamma \\ &\quad - (J_1 - J_2) \cos \beta \cos^2 \gamma - J_3 \cos \beta \dot{\beta} \\ c_{32} &= \frac{1}{2}((J_1 - J_2) \cos \beta \sin^2 \gamma - (J_1 - J_2) \cos \beta \cos^2 \gamma + J_3 \cos \beta) \dot{\alpha} \\ &\quad - ((J_1 - J_2) \cos \gamma \sin \gamma) \dot{\beta} \\ c_{33} &= 0 \end{aligned}$$

torque output [8]. Since the air-core coils are used in PMSA, the torque is linear to the current and can be expressed as

$$T = \begin{bmatrix} T_x \\ T_y \\ T_z \end{bmatrix} = GI \quad (6)$$

where the torque matrix G is $G = [G_1 \dots G_j \dots G_N]$, $G_j \in R^{3 \times 1}$ and the current input I is $I = [I_1 \dots I_j \dots I_N]^T$. Herein, the value of N is 15, for the coils can be divided into 15 groups. G_j describes the torque contribution of current on the j th coil, which is given as

$$G_j = \begin{cases} \sum_{i=1}^8 (-1)^{i-1} f(\varphi_{ij})(r_i \times s_j / |r_i \times s_j|), r_i \times s_j \neq 0 \\ 0, \quad r_i \times s_j = 0 \end{cases} \quad (7)$$

where $f(\varphi_{ij})$ is a torque function applicable to any pair of a PM pole and a coil obtained by curve fitting of the computed data using the finite element (FE) method and $\varphi_{ij} = \cos^{-1}(r_i \cdot s_j)$ is the separation angle between the PM pole and the coil.

It can be seen from (6) that the input contains 15 independent currents and the output includes three independent torques. Thus, there are redundant input currents which may be solved with the optimal control in order to minimise the total energy consumption for given torques. One such approach is to find I under the constraint of equation $T = GI$ in terms of minimising a quadratic cost function W defined as:

$$W = I^T RI \quad (8)$$

where R is a positive definite matrix in the form of

$$R = \text{diag}[R_1 \ R_2 \ \dots \ R_{15}]$$

where R_1, \dots, R_{15} are positive values determined by coils' resistances.

After introducing the Lagrangian multiplier $\lambda \in R^3$, the augmented cost function is given by

$$\bar{W} = I^T RI - \lambda^T (GI - T) \quad (9)$$

The optimal solution must satisfy

$$\begin{cases} \frac{\partial \bar{W}}{\partial I} = 2RI - G^T \lambda = 0 \\ \frac{\partial \bar{W}}{\partial \lambda} = T - GI = 0 \end{cases} \quad (10)$$

Solving for I yields

$$I = R^{-1} G^T (GR^{-1} G^T)^{-1} T \quad (11)$$

As all the coils have the same property and are arranged uniformly in the spherical motor, $R_i (i = 1, \dots, 15)$ can be normalised to 1 here. Hence, I can be transformed into the following equation:

$$I = G^T (GG^T)^{-1} T \quad (12)$$

In addition, it can be seen from the derivation process of G in [8] that G has linearly independent rows, which means G has full row rank. Thus, the existence of $(GG^T)^{-1}$ can be affirmed.

3 Robust dynamic decoupling control algorithm based on ADRC

The non-linearity and cross-couplings of the spherical motor are unmistakable by observing (5). Let

$$\begin{aligned} \theta_1 &= [\dot{\alpha}, \alpha] \\ \theta_2 &= [\dot{\beta}, \beta] \\ \theta_3 &= [\dot{\gamma}, \gamma] \\ w &= [w_\alpha, w_\beta, w_\gamma] \\ U &= [U_{\tau_\alpha}, U_{\tau_\beta}, U_{\tau_\gamma}] = \tau_c \end{aligned} \quad (13)$$

Equation (5) can be written as follows:

$$\begin{bmatrix} \ddot{\alpha} \\ \ddot{\beta} \\ \ddot{\gamma} \end{bmatrix} = \begin{bmatrix} f_1(\theta_1, \theta_2, \theta_3, w) \\ f_2(\theta_1, \theta_2, \theta_3, w) \\ f_3(\theta_1, \theta_2, \theta_3, w) \end{bmatrix} + \hat{M}(q)^{-1} \cdot \begin{bmatrix} U_{\tau_\alpha} \\ U_{\tau_\beta} \\ U_{\tau_\gamma} \end{bmatrix} \quad (14)$$

where α, β, γ are the output angles, w is the external disturbance and U is the actual control input torque.

Herein, we define $B(q) = \hat{M}(q)^{-1}$ as static couplings, since they are associated with the control law. Moreover, we define $f = [f_1, f_2, f_3]^T$ as dynamic couplings, since they are independent from the control law.

It is obvious that such two types of couplings should be resolved in different ways.

3.1 Reformulation of static decoupling control problem

By introducing the virtual control input

$$V = \hat{M}(q)^{-1} \cdot U = \begin{bmatrix} V_{\tau_\alpha} \\ V_{\tau_\beta} \\ V_{\tau_\gamma} \end{bmatrix} \quad (15)$$

(14) can be rewritten as

$$\begin{bmatrix} \ddot{\alpha} \\ \ddot{\beta} \\ \ddot{\gamma} \end{bmatrix} = \begin{bmatrix} f_1(\theta_1, \theta_2, \theta_3, w) \\ f_2(\theta_1, \theta_2, \theta_3, w) \\ f_3(\theta_1, \theta_2, \theta_3, w) \end{bmatrix} + \begin{bmatrix} V_{\tau_\alpha} \\ V_{\tau_\beta} \\ V_{\tau_\gamma} \end{bmatrix} \quad (16)$$

The above expression illustrates that three single input single output (SISO) subsystems have been obtained, which, respectively, describe the relationship between the output angles α, β, γ and the virtual input torques $V_{\tau_\alpha}, V_{\tau_\beta}, V_{\tau_\gamma}$.

In this way, corresponding ADRC controller can be constructed for each subsystem in an attempt to achieve conventional decoupling control in a square multi-variable system.

3.2 Reformulation of dynamic decoupling control problem

In PMSAs, the dynamic couplings between control loops as well as uncertainties can be treated as disturbances, which will be actively estimated and cancelled out in real time. As first shown in [27] for aircraft flight control and then in [30] for high performance of the turbofan engine, ADRC has been proved to be a natural solution to disturbance decoupling control in the presence of large uncertainties.

Equation (16) can be rewritten as a set of coupled input-output equations with predetermined input-output pairings.

$$\begin{cases} \ddot{\alpha} = f_1(\theta_1, \theta_2, \theta_3, w) + V_{\tau_\alpha} \\ \ddot{\beta} = f_2(\theta_1, \theta_2, \theta_3, w) + V_{\tau_\beta} \\ \ddot{\gamma} = f_3(\theta_1, \theta_2, \theta_3, w) + V_{\tau_\gamma} \end{cases} \quad (17)$$

Notably, $f_i (i = 1, 2, 3)$ represents the lumped disturbance of the i th loop, including combined effect of couplings and uncertainties.

The idea of ADRC is to estimate f_i in real time from the viable change in input-output information rather than by obtaining accurate mathematical description of f_i , which essentially breaks through the limitation of internal model principle and reduces the online computational work. Herein, ESO is proposed to realise above function.

3.3 Design of ESO

The ESO is designed for each channel independently. Instead of estimating f_i off-line, ESO can identify the lumped disturbance in real time.

For the sake of simplicity, we consider only one of three channels as follows, i.e. the motion of X -axis in (17)

$$\ddot{\alpha} = f_1(\theta_1, \theta_2, \theta_3, w) + V_{\tau_\alpha} \quad (18)$$

Let $x_{1,\alpha} = \alpha, x_{2,\alpha} = \dot{\alpha}$ and $x_{3,\alpha} = f_1$, which is added as an augmented state. Given that f_i is differentiable, we are able to define

$$h_1 = \frac{df_1}{dt} = \dot{f}_1 \quad (19)$$

Then, the subsystem (18) can be expressed in the state space form as

$$\begin{cases} \dot{x}_{1,\alpha} = x_{2,\alpha} \\ \dot{x}_{2,\alpha} = x_{3,\alpha} + V_{\tau_\alpha} \\ \dot{x}_{3,\alpha} = h_1 \\ y = x_{1,\alpha} \end{cases} \quad (20)$$

where $x_1 = [x_{1,\alpha} \ x_{2,\alpha} \ x_{3,\alpha}]^T \in R^3$ is the state vector.

Herein, f_1 is non-linear and time-varying, which seems to be hard for accurate modelling. Instead of finding an explicit analytical expression of f_1 , we design a classical third-order Luenberger observer, that is, the ESO, for the augmented state model (20) including f_1 . With the use of linear gains, we obtain the linear extended state observer (LESO) for the augmented state model, which not only gives good performance, but is also easy to tune [31–33]. According to (20), the LESO here can be expressed as

$$\begin{cases} e_{1,\alpha} = x_{1,\alpha} - \hat{x}_{1,\alpha} \\ \dot{\hat{x}}_{1,\alpha} = \hat{x}_{2,\alpha} + l_{1,\alpha} \cdot e_{1,\alpha} \\ \dot{\hat{x}}_{2,\alpha} = \hat{x}_{3,\alpha} + l_{2,\alpha} \cdot e_{1,\alpha} + V_{\tau_\alpha} \\ \dot{\hat{x}}_{3,\alpha} = l_{3,\alpha} \cdot e_{1,\alpha} \end{cases} \quad (21)$$

where $\hat{x}_1 = [\hat{x}_{1,\alpha} \ \hat{x}_{2,\alpha} \ \hat{x}_{3,\alpha}]^T \in R^3$ is the observed value of the state vector x_1 and $l_1 = [l_{1,\alpha} \ l_{2,\alpha} \ l_{3,\alpha}]^T$ is the gain parameter vector of the observer.

With a well-tuned ESO, the states obtained from the observer will closely track the states of the augmented system. This means that corresponding control strategy can cancel the effect of f_1 in real time using $x_{3,\alpha}$, i.e. $\hat{x}_{3,\alpha}$.

3.4 Design of controller

After the state observer has been properly designed, the controller can be constructed as

$$V_{\tau_\alpha} = -\hat{x}_{3,\alpha} + V_{\tau_{\alpha 0}} \quad (22)$$

Ignoring the estimation error in $x_{3,\alpha}$, the system is reduced to a unit gain double integration as

$$\ddot{\alpha} = (f_1 - \hat{x}_{3,\alpha}) + V_{\tau_{\alpha 0}} \approx V_{\tau_{\alpha 0}} \quad (23)$$

The control law is given by

$$V_{\tau_{\alpha 0}} = k_{1,\alpha}(r_\alpha - \hat{x}_{1,\alpha}) + k_{2,\alpha}(\dot{r}_\alpha - \hat{x}_{2,\alpha}) + \ddot{r}_\alpha \quad (24)$$

In general, the system can be easily controlled with a PD controller as below:

$$V_{\tau_{\alpha 0}} = k_p(r_\alpha - \hat{x}_{1,\alpha}) + k_d\hat{x}_{2,\alpha} \quad (25)$$

where $k_p = k_{1,\alpha}$, $k_d = k_{2,\alpha}$ and r_α is the given trajectory. Note that $k_d\hat{x}_{2,\alpha}$ instead of $k_d(\dot{r}_\alpha - \hat{x}_{2,\alpha})$, is used to avoid differentiation of the given trajectory and to make the closed-loop transfer function pure second order without a zero.

3.5 Parameterisation of ADRC

The LESO (21) and the matched controller (22) and (25) collaboratively constitute the linear active disturbance rejection control (LADRC), which is regarded as a special case of original ADRC. In other words, the LADRC uses linear gains in place of the non-linear ones in the observer and controller.

While the non-linear structure may be more effective, they also produce extra complexity in the parameter tuning and the proof of stability. Thus, the discussion in this paper is limited to the linear case, which offers us the opportunity to simplify the tuning process by introducing bandwidth parameterisation.

The bandwidth parameterisation can be used for designing both the observer and controller, which refers to assigning all eigenvalues at $\omega_{o,i}(i = \alpha, \beta, \gamma)$ or $\omega_{c,i}(i = \alpha, \beta, \gamma)$, then making all parameters of the observer and controller become a function of $\omega_{o,i}$ or $\omega_{c,i}$. Here, $\omega_{o,i}$ is the bandwidth of the observer and $\omega_{c,i}$ is the bandwidth of the controller. Since it is well known that bandwidth is closely linked to the performance of control system, the specifications of the design can be achieved by adjusting the value of $\omega_{o,i}$ or $\omega_{c,i}$.

Thus, as for ESO, the characteristic equation is chosen as

$$\lambda_{o,\alpha}(s) = s^3 + l_{1,\alpha}s^2 + l_{2,\alpha}s^2 + l_{3,\alpha} = (s + \omega_{o,\alpha})^3 \quad (26)$$

where

$$l_{1,\alpha} = 3\omega_{o,\alpha}, \quad l_{2,\alpha} = 3\omega_{o,\alpha}^2, \quad l_{3,\alpha} = \omega_{o,\alpha}^3 \quad (27)$$

This makes $\omega_{o,\alpha}$ the only tuning parameter of the observer. Generally, large bandwidth will increase the accuracy of estimation, whereas thin bandwidth will inhibit noise sensitivity. Hence, a compromise between tracking performance and noise tolerance should be considered.

As for the controller, the characteristic polynomial is obtained in the similar way as follows:

$$\lambda_{c,\alpha}(s) = s^2 + k_d s + k_p = (s + \omega_{c,\alpha})^2 \quad (28)$$

where

$$k_p = \omega_{c,\alpha}^2, \quad k_v = 2\omega_{c,\alpha} \quad (29)$$

In practice, the bandwidth $\omega_{c,\alpha}$ is tuned based on the requirements of performance as well as the noise sensitivity. Although a large controller bandwidth will bring fast response, it can also make the system oscillatory.

3.6 Convergence analysis

In this section, we firstly give the analysis of the convergence of the ESO in Theorem 1, in order to demonstrate that the estimated value of the state variable $\hat{x}_{j,\alpha}(t)(j = 1, 2, 3)$ can track the actual

value $x_{j,\alpha}(t)$ ($j = 1, 2, 3$) in definite time. Then, as the major work is to substitute the estimated value of the augmented state $\hat{x}_{3,\alpha}(t)$ into the state space equation, for the purpose of compensating the lumped disturbance, Theorem 2 is introduced to prove the stability of the closed-loop system, showing that the actual signal $x_{j,\alpha}(t)$ ($j = 1, 2$) can track the reference signal $r_{j,\alpha}(t)$ ($j = 1, 2$) in a finite time. The basic idea is as the following: first obtain the non-homogeneous state equation in terms of errors, then get the relationship between the error and time, and eventually prove the error to be bounded as time changes.

Since the introduction of virtual control input has separated the MIMO system into three SISO subsystems, in the following paragraph, we focus on the stability characteristics of a non-linear SISO system with couplings from other channels and various uncertainties. As the convergence analysis of three channels is similar, we only show the proof in the motion of X -axis.

As for the the convergence of the ESO, let $e_{j,\alpha}(t) = x_{j,\alpha}(t) - \hat{x}_{j,\alpha}(t)$, $j = 1, 2, 3$, that is,

$$\begin{cases} e_{1,\alpha} = x_{1,\alpha} - \hat{x}_{1,\alpha} \\ e_{2,\alpha} = x_{2,\alpha} - \hat{x}_{2,\alpha} \\ e_{3,\alpha} = x_{3,\alpha} - \hat{x}_{3,\alpha} \end{cases} \quad (30)$$

From (20), (21) and (27), we can obtain the tracking error dynamics

$$\begin{cases} \dot{e}_{1,\alpha} = e_{2,\alpha} - 3\omega_{0,\alpha}e_{1,\alpha} \\ \dot{e}_{2,\alpha} = e_{3,\alpha} - 3\omega_{0,\alpha}^2e_{1,\alpha} \\ \dot{e}_{3,\alpha} = h_1 - \omega_{0,\alpha}^3e_{1,\alpha} \end{cases} \quad (31)$$

Now we scale the observer tracking error as $\varepsilon_{j,\alpha}(t) = e_{j,\alpha}(t)/\omega_{0,\alpha}^{j-1}$, $j = 1, 2, 3$, that is,

$$\begin{cases} \varepsilon_{1,\alpha}(t) = e_{1,\alpha}(t) \\ \varepsilon_{2,\alpha}(t) = e_{2,\alpha}(t)/\omega_{0,\alpha} \\ \varepsilon_{3,\alpha}(t) = e_{3,\alpha}(t)/\omega_{0,\alpha}^2 \end{cases} \quad (32)$$

Then, (31) can be rewritten as

$$\dot{\varepsilon}_\alpha = \omega_{0,\alpha}A\varepsilon_\alpha + B\frac{h_1}{\omega_{0,\alpha}^2} \quad (33)$$

where $\varepsilon_\alpha = [\varepsilon_{1,\alpha}, \varepsilon_{2,\alpha}, \varepsilon_{3,\alpha}]^\top \in R^3$ is the state vector and

$$A = \begin{bmatrix} -3 & 1 & 0 \\ -3 & 0 & 1 \\ -1 & 0 & 0 \end{bmatrix}, \quad B = \begin{bmatrix} 0 \\ 0 \\ 1 \end{bmatrix} \quad (34)$$

Theorem 1: If h_1 is bounded, there exists a constant $\sigma > 0$ and a finite time $T_1 > 0$ so that $|e_{j,\alpha}(t)| \leq \sigma$, $j = 1, 2, 3$, $\forall t \geq T_1 > 0$ and $\omega_{0,\alpha} > 0$.

Proof: Solving the non-homogeneous equation (33), we can obtain one as

$$\varepsilon_\alpha(t) = e^{\omega_{0,\alpha}At}\varepsilon_\alpha(0) + \int_0^t e^{\omega_{0,\alpha}A(t-\tau)}B\frac{h_1}{\omega_{0,\alpha}^2}d\tau \quad (35)$$

First, Let

$$p_\alpha(t) = \int_0^t e^{\omega_{0,\alpha}A(t-\tau)}B\frac{h_1}{\omega_{0,\alpha}^2}d\tau \quad (36)$$

As h_1 is bounded, i.e. $|h_1| \leq \delta$, where δ is a positive constant. It is obvious that $p_\alpha = [p_{1,\alpha} \ p_{2,\alpha} \ p_{3,\alpha}]^\top \in R^3$ is a column vector, the element in each row of which has the following inequality, $j = 1, 2, 3$:

$$\begin{aligned} |p_{j,\alpha}(t)| &\leq \frac{\int_0^t [e^{\omega_{0,\alpha}A(t-\tau)}B]_j |h_1| d\tau}{\omega_{0,\alpha}^2} \\ &\leq \frac{\delta \int_0^t [e^{\omega_{0,\alpha}A(t-\tau)}B]_j d\tau}{\omega_{0,\alpha}^2} \\ &\leq \frac{\delta [A^{-1}(e^{\omega_{0,\alpha}At} - 1)B]_j}{\omega_{0,\alpha}^3} \\ &\leq \frac{\delta}{\omega_{0,\alpha}^3} \left(|[A^{-1}B]_j| + |[A^{-1}e^{\omega_{0,\alpha}At}B]_j| \right) \end{aligned} \quad (37)$$

From the definition of A , we can obtain

$$A^{-1} = \begin{bmatrix} 0 & 0 & -1 \\ 1 & 0 & -3 \\ 0 & 1 & -3 \end{bmatrix} \quad (38)$$

Hence

$$|[A^{-1}B]_j| = [0 \ 1 \ 3]^\top \leq 3 \quad (39)$$

According to (26), A is Hurwitz. Hence there exists a finite time $T_1 > 0$ so that

$$\left| [e^{\omega_{0,\alpha}At}]_{jk} \right| \leq \frac{1}{\omega_{0,\alpha}^2} \quad (40)$$

when $t \geq T_1$, $j = 1, 2, 3$. Hence,

$$\left| [e^{\omega_{0,\alpha}At}B]_j \right| \leq \frac{1}{\omega_{0,\alpha}^2}$$

when $t \geq T_1$, $j = 1, 2, 3$. Let

$$A^{-1} = \begin{bmatrix} s_{11} & s_{12} & s_{13} \\ s_{21} & s_{22} & s_{23} \\ s_{31} & s_{32} & s_{33} \end{bmatrix} \quad (41)$$

$$e^{\omega_{0,\alpha}At} = \begin{bmatrix} e_{11} & e_{12} & e_{13} \\ e_{21} & e_{22} & e_{23} \\ e_{31} & e_{32} & e_{33} \end{bmatrix} \quad (42)$$

Therefore,

$$\begin{aligned} \left| [A^{-1}e^{\omega_{0,\alpha}At}B]_j \right| &= \left| s_{j1}e_{13} + s_{j2}e_{23} + s_{j3}e_{33} \right| \\ &\leq \frac{|s_{j1}| + |s_{j2}| + |s_{j3}|}{\omega_{0,\alpha}^2} \\ &= \begin{cases} \frac{1}{\omega_{0,\alpha}^2} |s_{j1}| & j=1 \\ \frac{4}{\omega_{0,\alpha}^2} |s_{j2}| & j=2 \\ \frac{4}{\omega_{0,\alpha}^2} |s_{j3}| & j=3 \end{cases} \end{aligned} \quad (43)$$

when $t \geq T_1$, $j = 1, 2, 3$. We can deduce from (39) and (43) that

$$|p_{j,\alpha}(t)| \leq \frac{\delta}{\omega_{0,\alpha}^3} \left(3 + \frac{4}{\omega_{0,\alpha}^2} \right) \quad (44)$$

when $t \geq T_1, j = 1, 2, 3$.

Second, according to (40), the following inequality can be obtained:

$$\begin{aligned} \left| [e^{\omega_{0,\alpha}At} \varepsilon_\alpha(0)]_j \right| &= |e_{j1}\varepsilon_{1,\alpha}(0) + e_{j2}\varepsilon_{2,\alpha}(0) + e_{j3}\varepsilon_{3,\alpha}(0)| \\ &\leq \frac{|e_{1,\alpha}(0)| + |e_{2,\alpha}(0)| + |e_{3,\alpha}(0)|}{\omega_{0,\alpha}^{j+2}} \end{aligned} \quad (45)$$

From $\varepsilon_{j,\alpha}(t) = e_{j,\alpha}(t)/\omega_{0,\alpha}^{j-1}, j = 1, 2, 3$, we can get

$$\left| [e^{\omega_{0,\alpha}At} \varepsilon_\alpha(0)]_j \right| \leq \frac{|e_{1,\alpha}(0)| + |e_{2,\alpha}(0)| + |e_{3,\alpha}(0)|}{\omega_{0,\alpha}^{j+2}}$$

Let

$$|e_{\text{sum},\alpha}(0)| = |e_{1,\alpha}(0)| + |e_{2,\alpha}(0)| + |e_{3,\alpha}(0)| \quad (46)$$

It follows that

$$\left| [e^{\omega_{0,\alpha}At} \varepsilon_\alpha(0)]_j \right| \leq \frac{|e_{\text{sum},\alpha}(0)|}{\omega_{0,\alpha}^{j+2}}$$

Above all, from (35), we have

$$\begin{aligned} |\varepsilon_{j,\alpha}(t)| &\leq \left| [e^{\omega_{0,\alpha}At} \varepsilon_\alpha(0)]_j \right| + |p_{j,\alpha}(t)| \\ &\leq \frac{|e_{\text{sum},\alpha}(0)|}{\omega_{0,\alpha}^{j+2}} + \frac{\delta}{\omega_{0,\alpha}^3} \left(3 + \frac{4}{\omega_{0,\alpha}^2} \right) \end{aligned} \quad (47)$$

Therefore, we can further obtain

$$\begin{aligned} |e_{j,\alpha}(t)| &\leq \frac{|e_{\text{sum},\alpha}(0)|}{\omega_{0,\alpha}^3} + \frac{\delta}{\omega_{0,\alpha}^{4-j}} \left(3 + \frac{4}{\omega_{0,\alpha}^2} \right) \\ &\leq \frac{|e_{\text{sum},\alpha}(0)|}{\omega_{0,\alpha}^3} + \frac{3\delta}{\omega_{0,\alpha}^{4-j}} + \frac{4\delta}{\omega_{0,\alpha}^{7-j}} \end{aligned}$$

□

It is obvious that the tracking error of ESO can converge to a constant in the finite time, and the upper bound of the error monotonously decreases with the bandwidth of the observer. Generally speaking, a larger bandwidth will get more accurate estimation, whereas a smaller bandwidth will bring less noise. Thus, the selection of bandwidth should consider both two factors.

As for the convergence of the closed-loop system, we assume that the reference signal $r_{1,\alpha}(t)$, along with the derivatives of $r_{1,\alpha}(t)$, i.e. $\dot{r}_{1,\alpha}(t)$ and $\ddot{r}_{1,\alpha}(t)$, are bounded. Let

$$[r_{1,\alpha} \ r_{2,\alpha} \ r_{3,\alpha}]^\top = [r_\alpha \dot{r}_{1,\alpha} \ddot{r}_{1,\alpha}]^\top \quad (48)$$

Then we can definite $E_{j,\alpha}(t)$ as follows:

$$E_{j,\alpha}(t) = r_{j,\alpha}(t) - x_{j,\alpha}(t), \quad j = 1, 2 \quad (49)$$

That is,

$$\begin{cases} E_{1,\alpha}(t) = r_{1,\alpha}(t) - x_{1,\alpha}(t) \\ E_{2,\alpha}(t) = r_{2,\alpha}(t) - x_{2,\alpha}(t) \end{cases} \quad (50)$$

where $r_{j,\alpha}(t)$ is the reference signal and the $x_{j,\alpha}(t)$ is the actual signal.

Theorem 2: If h_1 is bounded, there exists a constant $\rho > 0$ and a finite time $T_3 > 0$ so that $|E_{j,\alpha}(t)| \leq \rho, j = 1, 2, 3, \forall t \geq T_3 > 0$, $\omega_{0,\alpha} > 0$ and $\omega_{c,\alpha} > 0$.

Proof: From (24), we can obtain

$$\begin{aligned} V_{\tau_\alpha} &= k_{1,\alpha}(r_{1,\alpha} - \hat{x}_{1,\alpha}) + k_{2,\alpha}(r_{2,\alpha} - \hat{x}_{2,\alpha}) + r_{3,\alpha} - \hat{x}_{3,\alpha} \\ &= k_{1,\alpha}[r_{1,\alpha} - (x_{1,\alpha} - e_{1,\alpha})] + k_{2,\alpha}[r_{2,\alpha} - (x_{2,\alpha} - e_{2,\alpha})] \\ &\quad - (x_{3,\alpha} - e_{3,\alpha}) + r_{3,\alpha} \\ &= k_{1,\alpha}(E_{1,\alpha} + e_{1,\alpha}) + k_{2,\alpha}(E_{2,\alpha} + e_{2,\alpha}) - (x_{3,\alpha} - e_{3,\alpha}) \\ &\quad + r_{3,\alpha} \end{aligned} \quad (51)$$

Let

$$E_\alpha = [E_{1,\alpha} \ E_{2,\alpha}]^\top \in R^2 \quad (52)$$

$$e_\alpha = [e_{1,\alpha} \ e_{2,\alpha} \ e_{3,\alpha}]^\top \in R^3 \quad (53)$$

Then, we have

$$\begin{aligned} \dot{E}_{1,\alpha} &= \dot{r}_{1,\alpha} - \dot{x}_{1,\alpha} = r_{2,\alpha} - x_{2,\alpha} = E_{2,\alpha} \\ \dot{E}_{2,\alpha} &= \dot{r}_{2,\alpha} - \dot{x}_{2,\alpha} = r_{3,\alpha} - (x_{3,\alpha} + V_{\tau_\alpha}) \\ &= -k_{1,\alpha}(E_{1,\alpha} + e_{1,\alpha}) - k_{2,\alpha}(E_{2,\alpha} + e_{2,\alpha}) - e_{3,\alpha} \end{aligned} \quad (54)$$

Hence we can obtain the state equation related to $E_{j,\alpha}$ as

$$\dot{E}_\alpha(t) = A_E E_\alpha(t) + A_e e_\alpha(t) \quad (55)$$

where

$$A_E = \begin{bmatrix} 0 & 1 \\ -k_{1,\alpha} & -k_{2,\alpha} \end{bmatrix} \quad (56)$$

$$A_e = \begin{bmatrix} 0 & 0 & 0 \\ -k_{1,\alpha} & -k_{2,\alpha} & -1 \end{bmatrix} \quad (57)$$

Solving the non-homogeneous (55), we can obtain one as

$$E_\alpha(t) = E^{A_E t} E_\alpha(0) + \int_0^t E^{A_E(t-\tau)} A_e e_\alpha(\tau) d\tau \quad (58)$$

According to (57), one has

$$\begin{aligned} |[A_e e_\alpha(\tau)]_{j=1,2}| &= 0 \\ |[A_e e_\alpha(\tau)]_{j=3}| &= |-k_{1,\alpha}e_{1,\alpha}(\tau) - k_{2,\alpha}e_{2,\alpha}(\tau) - e_{3,\alpha}(\tau)| \end{aligned} \quad (59)$$

From Theorem 1, we know there exist a constant $\sigma > 0$ and a finite time $T_1 > 0$ so that $|e_{j,\alpha}(t)| \leq \sigma, j = 1, 2, 3, \forall t \geq T_1 > 0$ and $\omega_{0,\alpha} > 0$. Hence

$$|[A_e e_\alpha(\tau)]_{j=3}| \leq (1 + k_{1,\alpha} + k_{2,\alpha})\sigma = \mu \quad (60)$$

Let

$$\phi_\alpha(t) = \int_0^t E^{A_E(t-\tau)} A_e e_\alpha(\tau) d\tau \quad (61)$$

and

$$\varphi = \begin{bmatrix} 0 \\ \mu \end{bmatrix} \quad (62)$$

It follows that

$$\begin{aligned} |\phi_{j,\alpha}(t)| &= \int_0^t [E^{A_E(t-\tau)} A_e e_\alpha(\tau)]_j d\tau \\ &\leq \int_0^t [E^{A_E(t-\tau)} \varphi]_j d\tau \\ &= [E^{A_E t} (-A_E^{-1}) E^{-A_E t}]_j \varphi \\ &= [E^{A_E t} (-A_E^{-1}) (E^{-A_E t} - 1)]_j \varphi \\ &= |[-A_E^{-1} \varphi]_j| + |[A_E^{-1} E^{A_E t} \varphi]_j| \end{aligned} \quad (63)$$

From the definition of A_E , we can obtain:

$$A_E^{-1} = \begin{bmatrix} -\frac{k_{2,\alpha}}{k_{1,\alpha}} & -\frac{1}{k_{1,\alpha}} \\ 1 & 0 \end{bmatrix} \quad (64)$$

According to (64), one has

$$\begin{aligned} |[A_E^{-1} \varphi]_1| &= \frac{\mu}{k_{1,\alpha}} = \frac{\mu}{\omega_{c,\alpha}^2} \\ |[A_E^{-1} \varphi]_2| &= 0. \end{aligned} \quad (65)$$

According to (28), A_E is Hurwitz. So there exist a finite time $T_2 > 0$ so that

$$|[E^{A_E t}]_{jk}| \leq \frac{1}{\omega_{c,\alpha}^3} \quad (66)$$

when $t \geq T_2, j = 1, 2$. Let

$$E^{A_E t} = \begin{bmatrix} o_{11} & o_{12} \\ o_{21} & o_{22} \end{bmatrix} \quad (67)$$

and $T_3 = \max\{T_1, T_2\}$, so we can obtain

$$|[E^{A_E t} \varphi]_j| \leq \frac{\mu}{\omega_{c,\alpha}^3} \quad (68)$$

when $t \geq T_3, j = 1, 2$. Thus

$$|[A_E^{-1} E^{-A_E t} \varphi]_j| \leq \begin{cases} \frac{1+k_{2,\alpha}}{k_{1,\alpha}} \frac{\mu}{\omega_{c,\alpha}^3} = \frac{1+k_{2,\alpha}}{\omega_{c,\alpha}^2} \frac{\mu}{\omega_{c,\alpha}^3}, & j = 1 \\ \frac{\mu}{\omega_{c,\alpha}^3}, & j = 2 \end{cases} \quad (69)$$

when $t \geq T_3, j = 1, 2$. According to (63), (65) and (69), we have

$$|\phi_{j,\alpha}(t)| \leq \begin{cases} \frac{\mu}{\omega_{c,\alpha}^2} + \frac{1+k_{2,\alpha}}{\omega_{c,\alpha}^2}, & j = 1 \\ \frac{\mu}{\omega_{c,\alpha}^3}, & j = 2 \end{cases} \quad (70)$$

Then we rewrite the $E^{A_E t} E_\alpha(0)$ as follows:

$$\begin{aligned} |[E^{A_E t} E_\alpha(0)]_j| &= |o_{j1} E_{1,\alpha}(0) + o_{j2} E_{2,\alpha}(0)| \\ &\leq |o_{j1} E_{1,\alpha}(0)| + |o_{j2} E_{2,\alpha}(0)| \\ &\leq \frac{|E_{1,\alpha}(0)| + |E_{2,\alpha}(0)|}{\omega_{c,\alpha}^3} \end{aligned} \quad (71)$$

Let

$$E_{\text{sum},\alpha}(0) = E_{1,\alpha}(0) + E_{2,\alpha}(0) \quad (72)$$

Hence

$$|[E^{A_E t} E_\alpha(0)]_j| \leq \frac{E_{\text{sum},\alpha}(0)}{\omega_{c,\alpha}^3} \quad (73)$$

From (58), one has

$$|E_{j,\alpha}(t)| \leq |[E^{A_E t} E_\alpha(0)]_j| + |\phi_{j,\alpha}(t)| \quad (74)$$

According to (70) and (73), we can obtain

$$|E_{j,\alpha}(t)| \leq \begin{cases} \frac{E_{\text{sum},\alpha}(0)}{\omega_{c,\alpha}^3} + \frac{\mu}{\omega_{c,\alpha}^2} + \frac{1+k_{2,\alpha}}{\omega_{c,\alpha}^2} \frac{\mu}{\omega_{c,\alpha}^3}, & j = 1 \\ \frac{E_{\text{sum},\alpha}(0) + \mu}{\omega_{c,\alpha}^3}, & j = 2 \end{cases} \quad (75)$$

$\leq \rho$

when $t \geq T_3, j = 1, 2$, where

$$\rho = \max \{|E_{1,\alpha}(t)|, |E_{2,\alpha}(t)|\}$$

□

It can be seen from above that the tracking error of angle and velocity can converge to a constant in the finite time, and the upper bound monotonously decreases with the bandwidth of the closed-loop system. Normally, a large bandwidth of the controller will bring the fast response. Nevertheless, it can also make the system oscillatory or even unstable. Hence, the controller bandwidth should be chosen in a compromise between the speed and stability.

4 Simulations

Simulations have been carried out for PMSA with the developed control strategy. The first simulation is aimed at evaluating how the coupling terms are compensated by ESO in the consideration of the model errors, as well as the load and random disturbance. Then, uncertainties are increased from 20 to 50% in order to evaluate the robustness of the proposed control algorithm.

In the second simulation, the nutation motion is introduced to verify the global controllability of PMSA as well as the improvement of both static and dynamic tracking performance.

The principal inertia moments of PMSA are obtained from automatic dynamic analysis of ADAMS with the solutions as $J_1 = 2.219 \text{ (kg} \cdot \text{m}^2)$, $J_2 = 2.176 \text{ (kg} \cdot \text{m}^2)$, $J_3 = 2.256 \text{ (kg} \cdot \text{m}^2)$.

4.1 Dynamic decoupling performance

The desired trajectory is

$$q = \begin{bmatrix} \alpha \\ \beta \\ \gamma \end{bmatrix} = \begin{bmatrix} \sin(\pi t) \\ \cos(\pi t) \\ 0.5 \end{bmatrix}, \quad t \in [0, 5]$$

The model uncertainties are set as follows:

$$\Delta M(q) = 0.2M(q), \quad \Delta C(\dot{q}, q) = 0.2C(\dot{q}, q)$$

where

$$\tilde{J}_1 = 1.2J_1, \quad \tilde{J}_2 = 1.2J_2, \quad \tilde{J}_3 = 1.2J_3$$

The external disturbances are set as follows:

$$\tau_d = \tau_l + \tau_r$$

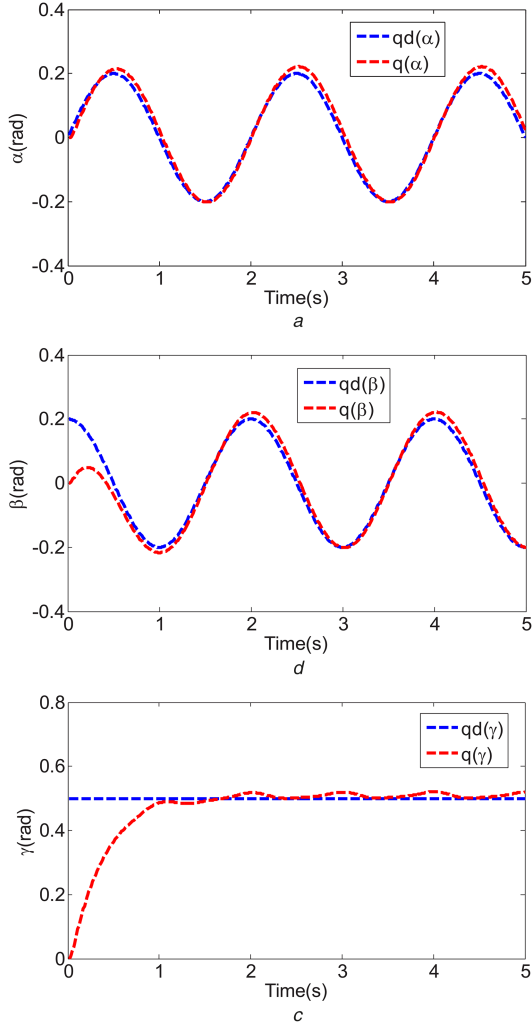


Fig. 3 Tracking performance with the PD control
(a) α angle, (b) β angle, (c) γ angle

where $\tau_l = [1, 1, 1]^T$ denotes the load torque and $\tau_r = 0.2r[\cos(\pi t), \sin(\pi t), \exp(-\pi t)]^T$ represents the random disturbance where r is randomly distributed in $(-1, 1)$. The above condition means that the system has 20% uncertainties, which include model errors and external disturbances.

The gains of PD controller are $k_p = \text{diag}[100, 100, 100]$ and $k_d = \text{diag}[40, 40, 40]$, whereas the tuned parameters for ADRC are $\omega_o = \text{diag}[30, 30, 30]$ and $\omega_c = \text{diag}[35, 35, 35]$.

Figs. 3 and 4 show the tracking performance of the given trajectory under the PD control method and the proposed control method, respectively. $qd(i)(i = \alpha, \beta, \gamma)$ denotes the desired output, and $q(i)(i = \alpha, \beta, \gamma)$ represents the actual output. The given signals of α and β change in sine form over time, while that of γ firstly reaches a certain angle and then stays unchanged. Fig. 3 shows that the angle of γ fluctuates around its desired value before dynamic decoupling, due to the effect of cross-couplings on γ , while Fig. 4 illustrates that the coupling terms from α and β has been significantly eliminated with the proposed control.

To valid the robustness of proposed control algorithm, the system uncertainties are greatly increased. The model uncertainties are set as follows:

$$\Delta M(q) = 0.5M(q), \quad \Delta C(\dot{q}, q) = 0.5C(\dot{q}, q)$$

where

$$\tilde{J}_1 = 1.5J_1, \quad \tilde{J}_2 = 1.5J_2, \quad \tilde{J}_3 = 1.5J_3$$

The external disturbances are set as follows:

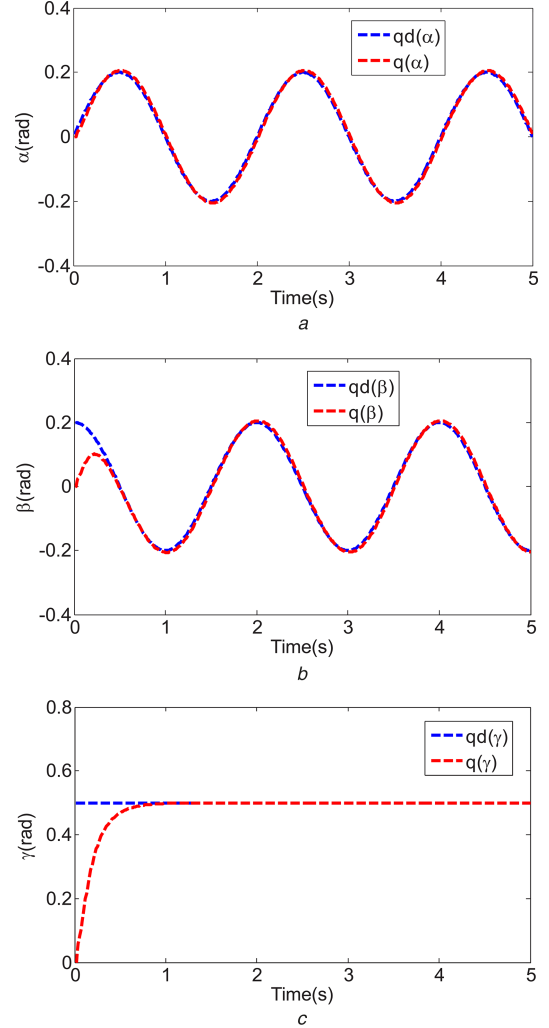


Fig. 4 Tracking performance with the proposed control
(a) α angle, (b) β angle, (c) γ angle

$$\tau_d = \tau_l + \tau_r$$

where $\tau_l = [1, 1, 1]^T$ denotes the load torque and $\tau_r = 0.5r[\cos(\pi t), \sin(\pi t), \exp(-\pi t)]^T$ represents the random disturbance where r is randomly distributed in $(-1, 1)$. The above condition means that the system has 50% uncertainties.

A comparison has been made in Figs. 5 and 6. Although the uncertainties involved in the lumped disturbance $f_i(i = 1, 2, 3)$, which contain the internal dynamics and external disturbance, respectively, have been largely increased, the ESO can still estimate accurately during the control process, so that the trajectory can fit the desired trajectory well, as shown in Fig. 6d.

4.2 Nutation motion

The nutation motion is similar to the motion of gyroscope, which can make a good inspection of global control ability. The system uncertainties are set as 20% and the desired trajectory is

$$q = \begin{bmatrix} \alpha \\ \beta \\ \gamma \end{bmatrix} = \begin{bmatrix} 0.2\sin(\pi t) \\ 0.2\cos(\pi t) \\ 2\pi t \end{bmatrix}, \quad t \in [0, 5]$$

The tracking performance under the PD and proposed control method is given in Figs. 7a and b, respectively. It can be clearly seen that there is an obvious steady-state error in the PD control strategy, illustrating that the internal disturbances which contain interactions among input-output pairs and model errors, along with the external disturbances which include the load and random disturbances, seriously influence the tracking performance. On the

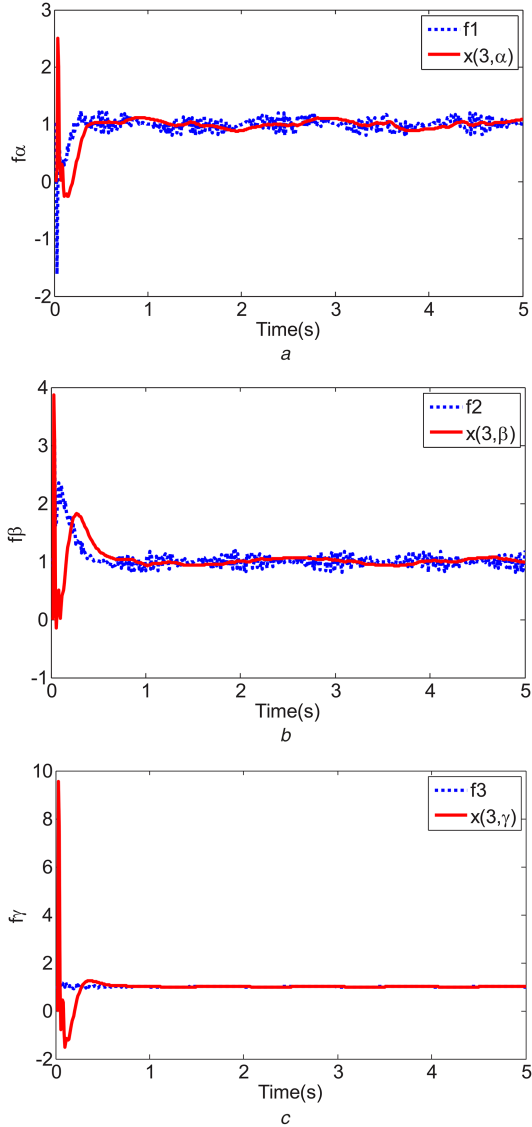


Fig. 5 Estimation of lumped disturbances with 20% uncertainties

(a) Estimation of lumped disturbance of α with 20% uncertainties, (b) Estimation of lumped disturbance of β with 20% uncertainties, (c) Estimation of lumped disturbance of γ with 20% uncertainties

contrast, in the proposed control strategy, since the real time identification of the above lumped disturbances is operated by the ESO, tracking errors in α , β and γ are smaller than the one. The result with little overshoot and no steady-state error demonstrates that both static and dynamic performance have been greatly improved.

5 Experiments

Experiments have been conducted to validate the proposed control method. Fig. 8a shows the experimental prototype of PMSA. The material of the rotor and stator shell is aluminum so as to eliminate the eddy current effect. The experimental platform is implemented by a personal computer (PC) and a current controller. A block diagram of the current controller consists of a digital signal processor (DSP), a field programmable gate array (FPGA), a AD5370, a V-I converting circuit and an orientation module (see Fig. 8b).

The DSP and FPGA constitute the core control module: the former one is responsible for task scheduling, communicating with the host computer and algorithm computing, and the latter one is in charge of driving the AD5370 chip and handling the data from the orientation module, as it features the ability of parallel processing. To generate bipolar currents in different channels simultaneously, the digital-to-analogue (D/A) chip AD5370 that can offer 40

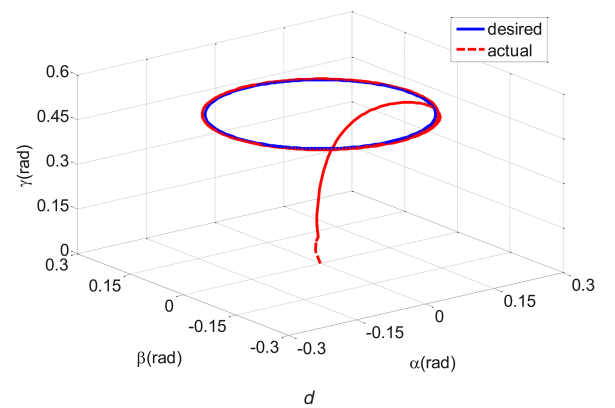
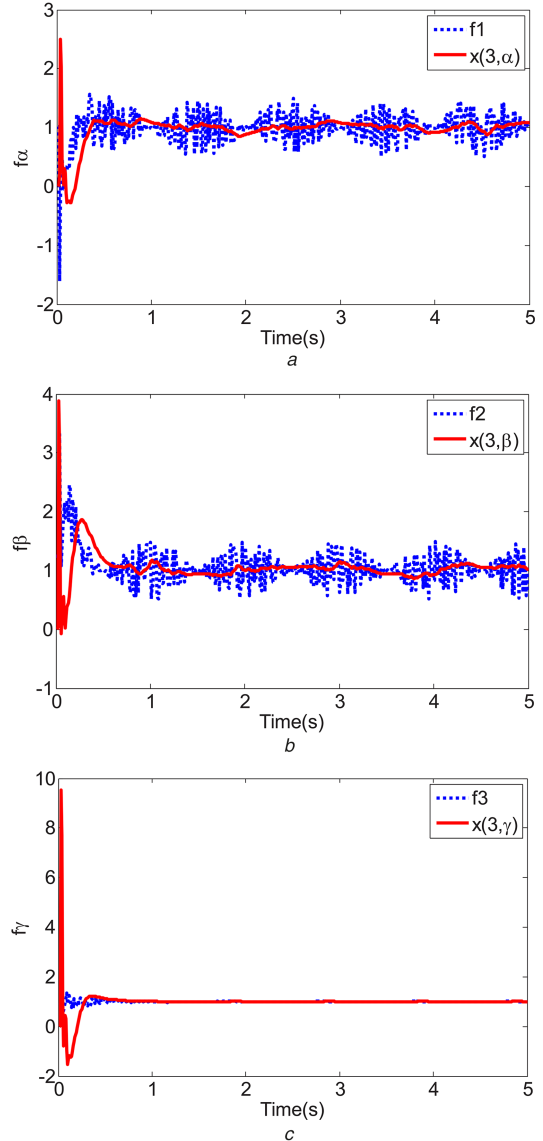


Fig. 6 Estimation of lumped disturbances and tracking performance with 50% uncertainties

(a) Estimation of lumped disturbance of α with 50% uncertainties, (b) Estimation of lumped disturbance of β with 50% uncertainties, (c) Estimation of lumped disturbance of γ with 50% uncertainties, (d) Tracking performance with 50% uncertainties

channels with 16-bit resolution D/A converting is used. Then, the V-I converting circuit can transform the voltage obtained from AD5370 into a proportional current.

A friendly graphical user interface program has been developed on the PC, which is employed to show the information about orientation and current and store the data for further analysis.

To observe the control performance conveniently, a typical trajectory along the X -axis of the rotor is conducted. In the

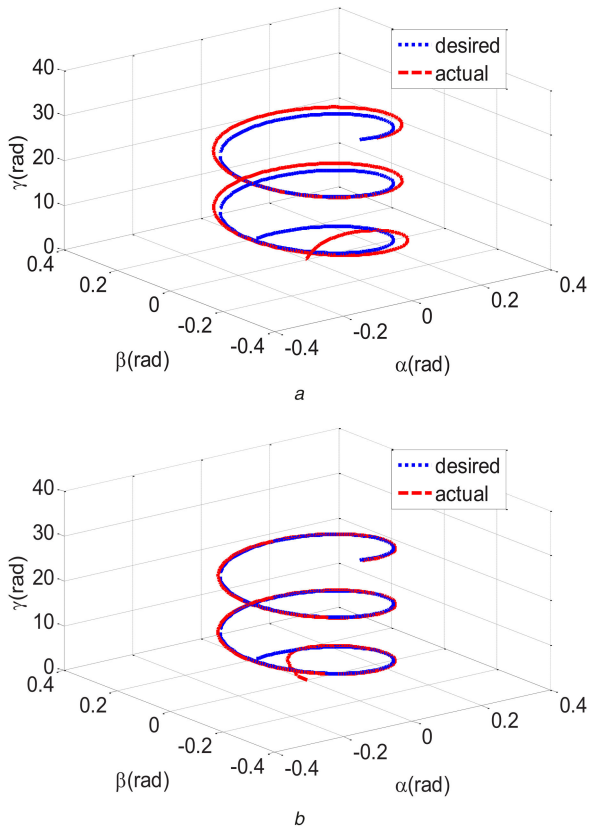


Fig. 7 Comparison of tracking performance under nutation motion

(a) Tracking performance under the PD control, (b) Tracking performance under the proposed control

experiment, a 0.1 kg mass of load is fixed to the output shaft. The rotor moves along the desired trajectory $q = [(\pi/60) \cdot t, 0, 0]^T$ for 3s and eventually stays at $q = [\pi/20, 0, 0]^T$.

Herein, a comparison is made about the control performance between the PD control and proposed control. It can be seen from Fig. 8c that although the given trajectory of Y-axis is 0, there still exists an undesirable deviation around the initial value, which should be attributed to the coupling effect from X-axis. Furthermore, an obvious steady-state error occurs in the X-axis during the control process, which denotes that the PD control scheme will be gravely affected when PMSA is subject to uncertainties, such as model errors and external disturbances. On the contrary, It can be observed in Fig. 8d that interactive influences of α and β has been estimated accurately using ESO and canceled out in the control law. Additionally, the actual trajectory fits the desired trajectory well with no steady-state error and overshoot in the X-axis, indicating that uncertainties, as part of the lumped disturbance, are effectively compensated as well.

It can be seen that compared with the PD control method, the proposed control algorithm can be viewed as a better choice for decoupling, which is also robust against various kinds of uncertainties. Meanwhile, a much better static and dynamic performance can be obtained in the actual system.

6 Conclusion

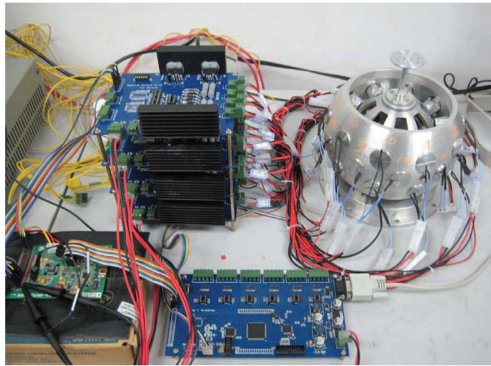
This paper analyses the robust dynamic decoupling control of PMSA in the presence of uncertainties. The non-linear dynamic model of PMSA with the interactions among various inputs and outputs has been established based on the Lagrange's equation, and the torque model has been formulated by FE analysis and curve fitting method. Since PMSA is a multi-variable non-linear system with strong couplings, it is necessary to introduce the concept of virtual control input, in an attempt to eliminate the static couplings among input-output pairs and partition such MIMO system into three SISO subsystems. Nevertheless, the above SISO system is not independent from each other, hence the effect of one input to all other outputs that is not paired with should be viewed as

disturbances. It is obvious that ADRC is a natural solution in this case. As the core part of the decoupling control system, ESO has been chosen as the observer, which requires little information of the disturbance. What sets ESO apart from others is that it can estimate not only the internal dynamics but also the external disturbance. Notably, the non-linear structure of ESO with a large number of tuning parameters limits its application in practice. Hence, the linear one has been selected instead, which makes it possible to simplify the tuning process by introducing the method of bandwidth parameterisation. It refers to assigning all observer eigenvalues at the bandwidth, of which all parameters of ESO is a function. Besides, the same method is employed for the design of the controller as well. Finally, simulations have validated that this control strategy can effectively eliminate the influence of cross-couplings in PMSAs as well as uncertainties. In addition, both the static and dynamic decoupling performances have been greatly improved with strong robustness. The subsequent experiments have also verified the validity of the proposed algorithm.

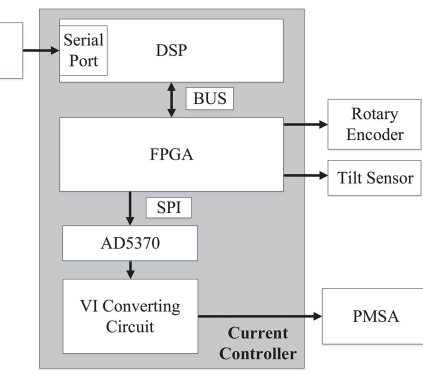
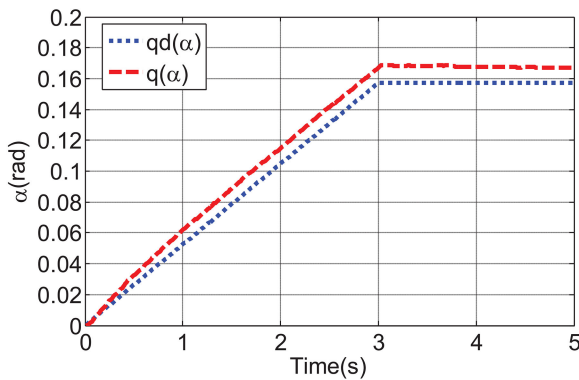
LADRC offers the opportunity to simplify the process of tuning parameters. Nevertheless, the linear form of ADRC seems to be less competitive compared with the non-linear one in some aspects, such as relatively lower control power and possibility of parameter's overflowing. Thus, in order to apply PMSA to more complicated situation, the future work could focus on how to solve the problems existing in the non-linear form of ADRC, such as the selection of parameters and non-linear functions.

8 Acknowledgments

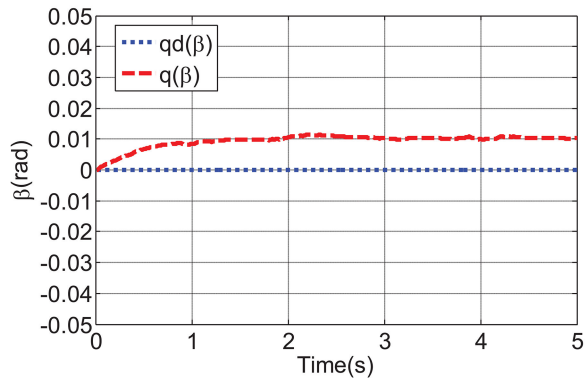
This work was supported by National Natural Science Foundation of China under Project 51475033 and 51475017 and by Beijing Municipal Natural Science Foundation under Project 3152018.



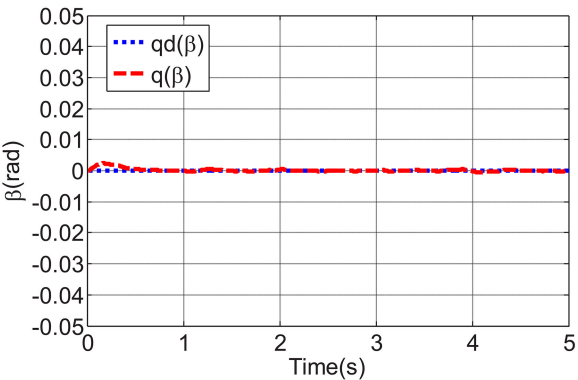
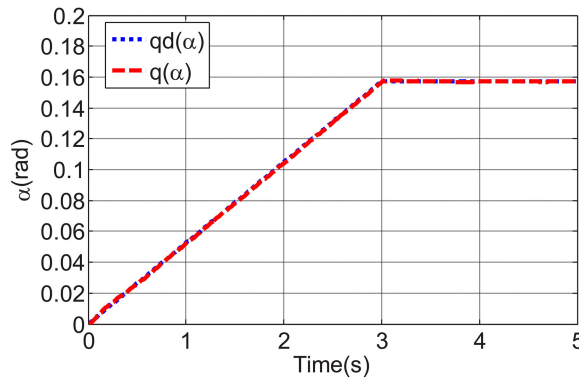
a



b



c



d

Fig. 8 Experimental results under different control methods

(a) Experimental prototype of PMSA, (b) Block diagram of the control system, (c) Tracking performance under the PD control, (d) Tracking performance under the proposed control

9 References

- [1] Toyama, S., Sugitani, S., Guoqiang, Z., *et al.*: 'Multi degree of freedom spherical ultrasonic motor'. Proc. 1995 IEEE Int. Conf. on Robot. Autom., 1995, Vol. 3, pp. 2935–2940
- [2] Shigeki, T., Guoqiang, Z., Osamu, M.: 'Development of new generation spherical ultrasonic motor'. Proc. 1996 IEEE Int. Conf. on Robot. Autom., 1996, Vol. 3, pp. 2871–2876
- [3] Lee, K.-M., Kwan, C.-K.: 'Design concept development of a spherical stepper for robotic applications', *IEEE Trans. Robot. Autom.*, 1991, **7**, (1), pp. 175–181
- [4] Son, H., Lee, K.-M.: 'Open-loop controller design and dynamic characteristics of a spherical wheel motor', *IEEE Trans. Ind. Electron.*, 2010, **57**, (10), pp. 3475–3482
- [5] Wang, J., Wang, W., Jewell, G.W., *et al.*: 'A novel spherical permanent magnet actuator with three degrees-of-freedom', *IEEE Trans. Magn.*, 1998, **34**, (4), pp. 2078–2080
- [6] Xia, C., Li, H., Shi, T.: '3-d magnetic field and torque analysis of a novel Halbach array permanent-magnet spherical motor', *IEEE Trans. Magn.*, 2008, **44**, (8), pp. 2016–2020
- [7] Xia, C., Song, P., Li, H., *et al.*: 'Research on torque calculation method of permanent-magnet spherical motor based on the finite-element method', *IEEE Trans. Magn.*, 2009, **45**, (4), pp. 2015–2022
- [8] Chen, W., Zhang, L., Yan, L., *et al.*: 'Design and control of a three degree-of-freedom permanent magnet spherical actuator', *Sens. Actuators A Phys.*, 2012, **180**, pp. 75–86
- [9] Bai, K., Lee, K.-M.: 'Direct field-feedback control of a ball-joint-like permanent-magnet spherical motor', *IEEE/ASME Trans. Mechatron.*, 2014, **19**, (3), pp. 975–986
- [10] Son, H., Lee, K.-M.: 'Control system design and input shape for orientation of spherical wheel motor', *Control Eng. Pract.*, 2014, **24**, pp. 120–128
- [11] Guo, W., Yang, J., Yang, W., *et al.*: 'Regulation quality for frequency response of turbine regulating system of isolated hydroelectric power plant with surge tank', *Int. J. Electr. Power Energy Syst.*, 2015, **73**, pp. 528–538
- [12] Guo, W., Yang, J., Wang, M., *et al.*: 'Nonlinear modeling and stability analysis of hydro-turbine governing system with sloping ceiling tailrace tunnel under load disturbance', *Energy Convers. Manag.*, 2015, **106**, pp. 127–138
- [13] Guo, W., Yang, J., Chen, J., *et al.*: 'Nonlinear modeling and dynamic control of hydro-turbine governing system with upstream surge tank and sloping ceiling tailrace tunnel', *Nonlinear Dyn.*, 2016, **84**, (3), pp. 1383–1397
- [14] Lee, K.-M., Roth, R.B., Zhou, Z.: 'Dynamic modeling and control of a ball-joint-like variable-reluctance spherical motor', *J. Dyn. Syst. Meas. Control*, 1996, **118**, (1), pp. 29–40
- [15] Wang, W., Wang, J., Jewell, G., *et al.*: 'Design and control of a novel spherical permanent magnet actuator with three degrees of freedom', *IEEE/ASME Trans. Mechatron.*, 2003, **8**, (4), pp. 457–468
- [16] Xia, C., Guo, C., Shi, T.: 'A neural-network-identifier and fuzzy-controller-based algorithm for dynamic decoupling control of permanent-magnet spherical motor', *IEEE Trans. Ind. Electron.*, 2010, **57**, (8), pp. 2868–2878
- [17] Chu, J., Niguchi, N., Hirata, K.: 'Feedback control of outer rotor spherical actuator using adaptive neuro-fuzzy inference system'. 2013 Seventh Int. Conf. IEEE Sens. Technol. (ICST), 2013, pp. 401–405

- [18] Zhang, L., Chen, W., Liu, J., *et al.*: ‘A robust adaptive iterative learning control for trajectory tracking of permanent-magnet spherical actuator’, *IEEE Trans. Ind. Electron.*, 2016, **63**, (1), pp. 291–301
- [19] Su, J., Qiu, W., Ma, H., *et al.*: ‘Calibration-free robotic eye-hand coordination based on an auto disturbance-rejection controller’, *IEEE Trans. Robot.*, 2004, **20**, (5), pp. 899–907
- [20] Su, J., Ma, H., Qiu, W., *et al.*: ‘Task-independent robotic uncalibrated hand-eye coordination based on the extended state observer’, *IEEE Trans. Syst. Man Cybern. B Cybern.*, 2004, **34**, (4), pp. 1917–1922
- [21] Su, Y.X., Zheng, C.H., Duan, B.Y.: ‘Automatic disturbances rejection controller for precise motion control of permanent-magnet synchronous motors’, *IEEE Trans. Ind. Electron.*, 2005, **52**, (3), pp. 814–823
- [22] Li, S., Liu, Z.: ‘Adaptive speed control for permanent-magnet synchronous motor system with variations of load inertia’, *IEEE Trans. Ind. Electron.*, 2009, **56**, (8), pp. 3050–3059
- [23] Li, S., Yang, X., Yang, D.: ‘Active disturbance rejection control for high pointing accuracy and rotation speed’, *Automatica*, 2009, **45**, (8), pp. 1854–1860
- [24] Xia, Y., Zhu, Z., Fu, M., *et al.*: ‘Attitude tracking of rigid spacecraft with bounded disturbances’, *IEEE Trans. Ind. Electron.*, 2011, **58**, (2), pp. 647–659
- [25] Wang, J., Ma, H., Cai, W., *et al.*: ‘Research on micro quadrotor control based on adrc’, *J. Projectiles Rockets, Missiles Guid.*, 2008, **3**, p. 008
- [26] Gong, X., Tian, Y., Bai, Y., *et al.*: ‘Trajectory tracking control of a quad-rotor based on active disturbance rejection control’, 2012 IEEE Int. Conf. IEEE Autom. Logist. (ICAL), 2012, pp. 254–259
- [27] Huang, Y., Xu, K., Han, J., *et al.*: ‘Flight control design using extended state observer and non-smooth feedback’. Proc. IEEE Conf. on Decision and Control, 2001, Vol. 1, pp. 223–228, available at: <http://www.ieeecss.org>
- [28] Zheng, Q., Chen, Z., Gao, Z.: ‘A practical approach to disturbance decoupling control’, *Control Eng. Pract.*, 2009, **17**, (9), pp. 1016–1025
- [29] Hall, C.E., Shtessel, Y.B.: ‘Sliding mode disturbance observer-based control for a reusable launch vehicle’, *J. Guid. Control Dyn.*, 2006, **29**, (6), pp. 1315–1328
- [30] Miklosovic, R., Gao, Z.: ‘A dynamic decoupling method for controlling high performance turbofan engines’. Proc. of the 16th IFAC World Congress, 2005, pp. 4–8
- [31] Gao, Z.: ‘Scaling and bandwidth-parameterization based controller tuning’. Proc. American Control Conf., 2006, vol. 6, pp. 4989–4996
- [32] Gao, Z.: ‘Active disturbance rejection control: a paradigm shift in feedback control system design’. 2006 IEEE American Control Conf., 2006, 7pp
- [33] Zheng, Q., Gao, L.Q., Gao, Z.: ‘On validation of extended state observer through analysis and experimentation’, *J. Dyn. Syst. Meas. Control*, 2012, **134**, (2), p. 024505